



# Preparation and characterization of 1-ethyl-3-methylimidazolium chloride-based gel polymer electrolyte in electrochemical double-layer capacitors

R. M. L. L. Rathnayake<sup>1</sup> · K. S. Perera<sup>1</sup> · K. P. Vidanapathirana<sup>1</sup>

Received: 19 March 2020 / Revised: 20 June 2020 / Accepted: 6 July 2020 / Published online: 10 July 2020  
© Springer-Verlag GmbH Germany, part of Springer Nature 2020

## Abstract

Electrochemical double-layer capacitors (EDLCs) have recently received an enormous attraction due to their ability to produce higher power density without compromising the durability. Producing cheaper, safer, and more durable devices obviously brings more benefits to the modern world applications. This investigation was carried out to optimize an ionic liquid (IL)-based gel polymer electrolyte (GPE), to fabricate an EDLC using the optimized electrolyte with natural graphite electrodes, and to characterize the performance of the device. Electrolyte was prepared with the IL, 1-ethyl-3-methylimidazolium chloride (1E3MCl); the polymer poly(vinylidene fluoride)-co-hexafluoropropylene (PVdF-co-HFP); and the salt, zinc chloride (ZnCl<sub>2</sub>). The electrochemical properties of the electrolyte were evaluated by electrochemical impedance spectroscopy (EIS), DC polarization test, and linear sweep voltammetry (LSV), and the EDLC was characterized by EIS, cyclic voltammetry (CV), and galvanostatic charge–discharge (GCD) test. The optimum composition was found to be 26% PVdF-co-HFP:52% ZnCl<sub>2</sub>:22% 1E3MCl (weight percentages) with the room temperature conductivity of  $1.85 \times 10^{-3} \text{ S cm}^{-1}$  and ionic transference number of 0.72. EDLC exhibited a single-electrode specific capacitance of  $4.92 \text{ F g}^{-1}$  with 65% retention over 1000 cycles as per CV test. In the GCD results, the EDLC was able to hold discharge capacitance of  $3 \text{ F g}^{-1}$  for complete 1000 cycles. The durability of the EDLC with this IL-based GPE shows a great potential in the energy applications with further enhancements.

**Keywords** Ionic liquid · Gel polymer electrolytes · Electrochemical double-layer capacitors (EDLCs) · 1-Ethyl-3-methylimidazolium chloride · Graphite electrodes · Poly(vinylidene fluoride)-co-hexafluoropropylene (PVdF-co-HFP)

## Introduction

Depletion of fossil fuel as well as the swift increase of energy demand forced people to think about renewable energy sources more and more. To continuously fulfill the energy demand, energy storage devices have become an essential component in such an infrastructure. Therefore, producing high performing energy storage devices has gained a lot of interest among the researchers worldwide. One of the major approaches for this is producing highly efficient electrolytes. Development of polymer electrolytes (PEs) drew the attention as they find applications in lithium batteries as well as in other

electrochemical devices such as supercapacitors [1]. These polymer electrolytes have several advantages over their liquid counterparts such as no internal shorting, leakage of electrolytes, and non-combustible reaction products at the electrode surface existing in the liquid electrolytes. To avoid majority of these problems while keeping the advantages of liquid electrolytes, “gel polymer electrolytes (GPEs)” which are neither liquid nor solid have been suggested. GPEs possess both cohesive properties of solids and the diffusive properties of liquids. In addition, they exhibit higher conductivity than conventional PEs. These unique characteristics make them suitable to consider for various important applications [2, 3].

GPEs are mainly consisting with a salt/solvent mixture encapsulated with a polymer host [4]. But these organic solvents are well famous for their toxicity. In addition, they carry some major demerits such as volatility and flammability. Ionic liquids (ILs) have emerged as one of the promising substitutions to organic solvents currently in high energy density devices. They have the ability to add superior properties such as

✉ K. S. Perera  
kumudu31966@gmail.com

<sup>1</sup> Department of Electronics, Wayamba University of Sri Lanka, Kuliyaipitiya, Sri Lanka

higher potential tolerance, faster ion transference rate, higher ionic transference number, and the good retention caused by the low vapor pressure in operating temperatures which are most of time staying below 100 °C [5]. On the other hand, cost-effective reliable electrodes may also play the counterpart of the electrolyte to produce the improvement in devices. As a substitute for the traditional expensive and less safe electrodes, graphite-based electrodes have been identified due to their outstanding properties such as the higher surface area for a unit mass, minimum electrochemical reaction rate, good mechanical stability, and the higher conductivity without compromising the less complicated procedure of appliance in addition to the higher natural abundance. Chemical deposition on the graphite layers is also minimal compared with the other substances. Therefore, graphite electrodes are extremely beneficial for the devices which are optimized for higher power densities [6]. Supercapacitors are notable for their high power density and quick charge–discharge capability with considerable amount of energy density which is an important property of a device that needs quick burst of energy for a brief period of time such as for accelerating an electric vehicle [7].

In this study, IL-based GPEs were prepared with 1-ethyl-3-methylimidazolium chloride (1E3MICl), zinc chloride ( $\text{ZnCl}_2$ ), and poly(vinylidene fluoride-co-hexafluoropropylene) (PVdF-co-HFP). Conductivity of the system was optimized by varying the composition. GPE was characterized by DC polarization test and the linear sweep voltammetry (LSV) test. Then, the GPE with the optimum conductivity was used to fabricate electrochemical double-layer capacitors (EDLCs) with Sri Lankan natural graphite as the electrodes, and they were characterized using electrochemical impedance spectroscopy (EIS), cyclic voltammetry (CV), and galvanostatic charge–discharge (GCD) test.

## Methodology

### Preparation of gel polymer electrolytes

Suitable amount of PVdF-co-HFP (average  $M_w \sim 40000$ , Sigma-Aldrich) was dissolved in acetone with magnetic stirring.  $\text{ZnCl}_2$  (98%, Sigma-Aldrich) and 1E3MICl (95%, Sigma-Aldrich) were added later into the solution and continuously stirred until a homogeneous blend was obtained. Then, the resultant transparent mixture was poured in to a well-cleaned petri dish and the solvent was left to evaporate. Thereby, a bubble-free, uniform, mechanically stable thin film was obtained.

### AC conductivity measurements

A circular piece of the sample was separated and sealed in between two stainless steel (SS) electrodes in a spring-

loaded sample holder. Impedance data were collected in between the frequency range 0.1 Hz to 400 kHz with a Metrohm impedance analyzer (M101) for different temperatures within 28 to 55 °C. Then, the composition of GPE was optimized to obtain the highest value for the conductivity. It was selected to continue with further characterization.

Conductivity ( $\sigma$ ) of the electrolyte was calculated by:

$$\sigma = \left( \frac{1}{R_b} \right) \times \left( \frac{t}{A} \right)$$

where  $R_b$  is the bulk resistance of electrolyte,  $t$  is the thickness, and  $A$  is the area of cross section of the electrolyte film [8].

### Transference number measurements

A circular-shaped sample was separated from the film and sandwiched in between two SS electrodes. Then, a constant potential was applied while measuring the current through the electrolyte with time. The ionic transference number ( $t_i$ ) was calculated using the equation with the DC polarization test results:

$$t_i = \frac{(I_i - I_o)}{I_i}$$

where  $I_i$  is the initial current and  $I_o$  is the stable current [9].

### Electrochemical stability window

Electrochemical stability window decides the stable potential range of charge and discharge of an electrolyte. Linear sweep voltammetry (LSV) test was carried out with SS/IL-based GPE/Zn electrode electrolyte configuration to find the electrochemical stability window of the electrolyte. Current through the system was measured using a potentiostat (Metrohm M101).

### Preparation of graphite electrode

Natural graphite was obtained from Bogala Graphite Lanka Ltd., Sri Lanka, and ultrasonic homogenizer was used to sonicate graphite with acetone in ambient temperature to form a homogeneous paste. Then, the paste was applied thoroughly on two cleaned fluorine-doped tin oxide (FTO) glass plates with a surface area of 1  $\text{cm}^2$ . The mass of a single electrode was measured using an electronic balance (Radwag).

### Fabrication and characterization of EDLC

The EDLC was fabricated with an IL-based GPE sandwiched within a pair of graphite electrodes.

Electrochemical impedance spectroscopy (EIS) test for the EDLC was performed with Metrohm Autolab Impedance

Analyzer M101 at ambient temperature. The real ( $C'(\omega)$ ) and imaginary ( $C''(\omega)$ ) parts of the complex capacitances were calculated from the complex impedance of the system as below.

$$C'(\omega) = \frac{Z''(\omega)}{\omega|Z(\omega)|^2}$$

$$C''(\omega) = \frac{Z'(\omega)}{\omega|Z(\omega)|^2}$$

where  $Z(\omega)$  is the complex impedance with  $Z'(\omega)$  and  $Z''(\omega)$  being the real and the imaginary parts, respectively.  $\omega = 2\pi f$  where  $f$  is the frequency [10].

Cyclic voltammetry (CV) test was done in various potential windows, and thereby, the optimum window was chosen with the highest single-electrode specific capacitance ( $C_{sc}$ ) value. It was used to find the optimum scanning rate of the system. The continuous CV test was done for 1000 cycles.  $C_{sc}$  was calculated through:

$$C_{sc} = 2(\int IdV) / \Delta VSm$$

where  $\int IdV$  is the area under cyclic voltammograms,  $m$  is the mass of a single electrode,  $S$  is the scan rate, and  $\Delta V$  is the applied potential window [11].

Galvanostatic charge–discharge (GCD) test was done within 0.1–0.9 V range with a constant current of 0.1 mA using the Metrohm impedance analyzer to obtain the single-electrode specific discharge capacitance ( $C_{sd}$ ) of the EDLC.

$$C_{sd} = \frac{I}{m \left( \frac{dv}{dt} \right)}$$

where  $I$  is the current,  $m$  is the mass of a single electrode, and  $dv/dt$  is the drop rate of the potential (excluding  $IR$  drop of discharge).

## Results and discussion

### Optimizing the electrolyte

EIS tests were carried out over a frequency range of 0.1 to 400 kHz, and the Nyquist plot of one of the electrolytes investigated at 28 °C is shown in Fig. 1.

Nyquist plots represent the imaginary versus the real parts of the complex impedance of individual electrodes. The  $R_b$  of the polymer electrolyte can be obtained from the intercept on the real axis of the Nyquist plot. In this work, the semi-circular portions corresponding to the high-frequency region are absent, indicating that the majority of the current carriers in the electrolyte medium are ions. The obtained inclined spike

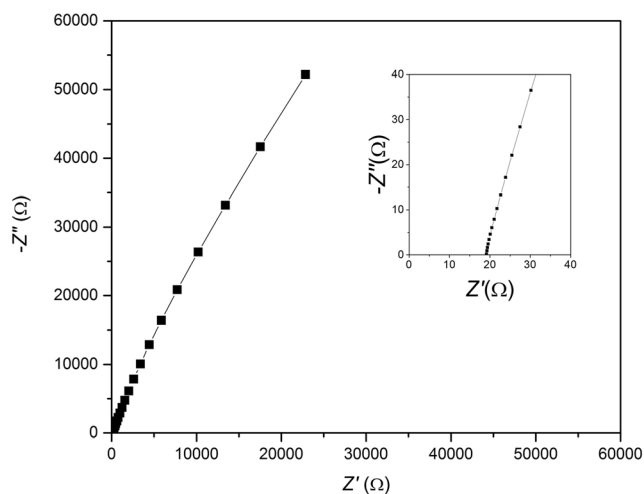


Fig. 1 The Nyquist plot of one of the electrolyte investigated compositions at 28 °C

corresponding to the lower-frequency region is due to double-layer capacitance in a cell with an ion-blocking electrode (SS) configuration [12].

Impedance data was used to calculate the conductivity of the electrolytes. Figure 2 shows the ambient temperature (28 °C) conductivity variation with respect to the IL weight percentage.

Conductivity increased with the IL concentration, and the value of conductivity began to drop after the IL concentration reached 22 weight percentage. This concludes that the optimum conductivity in the room temperature of  $1.85 \times 10^{-3} \text{ S cm}^{-1}$  can be obtained from the composition of 26% PVdF-co-HFP:52%  $\text{ZnCl}_2$ :22% 1E3MICl weight percentages. Also, the samples with higher IL concentrations than 25 weight percentage began to deform and a clear separation among materials was observed on the membranes.

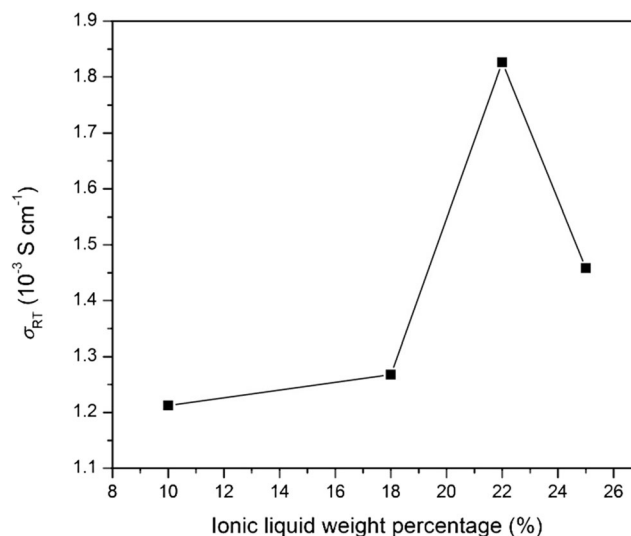


Fig. 2 Room temperature conductivity ( $\sigma_{RT}$ ) variation with respect to the IL (weight percentage)

Ionic conductivity ( $\sigma$ ) is dependent on ion concentration ( $n$ ) and the mobility of the ions ( $\mu$ ) as given by:

$$\sigma = ne\mu$$

where  $e$  is the charge. A possible reason for the initial enhancement of ionic conductivity is the increase of the concentration of mobile charge species with the increase IL concentration. The ionic conductivity began to decrease after IL concentration reached 22% in weight. It may be caused by the dominant effect of viscosity of the medium that limits the ionic mobility. In addition to that, at higher charged ion concentrations, the mobility decreases due to the formation of ion agglomerates [13].

### Conductivity variation with the temperature

A substantial increment of ionic conductivity can be seen with the temperature as a general trend. When temperature increases, ions become thermally energetic and their mobility increases. In addition, with the temperature increase, viscosity decreases resulting in higher mobility. These all contribute finally for the conductivity escalation [14]. However, variation of conductivity with temperature differs from one system to another. It is because there are two main conducting mechanisms that govern the conductivity temperature behavior in different systems. They are the Arrhenius behavior and Vogel-Tamman-Fulcher behavior.

#### i. Arrhenius behavior

$$\sigma = \sigma_0 \exp\left(-\frac{E_a}{k_B T}\right)$$

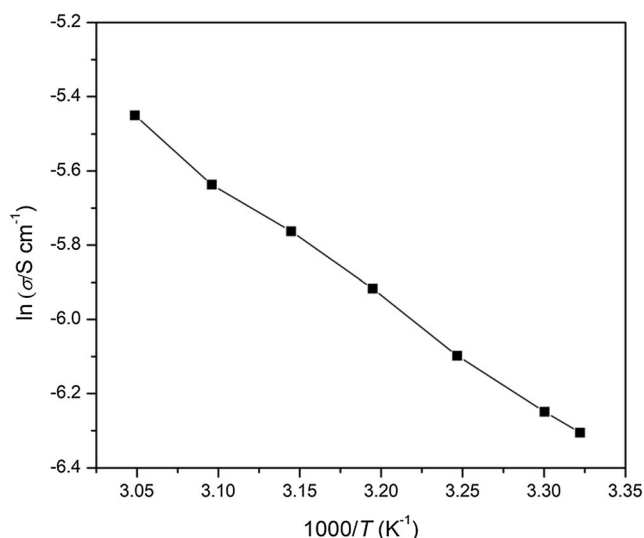


Fig. 3  $\ln(\sigma/S\text{ cm}^{-1})$  values with respect to the  $1000/T$

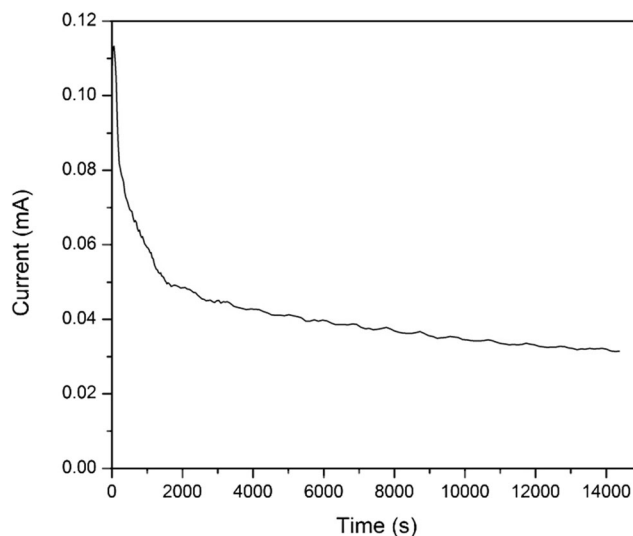


Fig. 4 Resulted DC polarization plot for the blocking electrodes

where  $k_B$  is the Boltzmann constant.  $E_a$  is the activation energy. Here, ion conduction is assumed to be taken place via hopping of ions in between coordination sites. The graph of  $\ln(\sigma/S\text{ cm}^{-1})$  versus  $1000/T$  takes the form of a straight line if a particular system behaves according to the Arrhenius behavior.

#### ii. Vogel-Tamman-Fulcher (VTF) behavior

$$\sigma = AT^{-\frac{1}{2}} \exp\left(\frac{E_a}{k_B(T-T_0)}\right)$$

where  $A$  is an exponential factor,  $E_a$  is the activation energy,  $k_B$  is the Boltzmann constant, and  $T_0$  is the equilibrium glass transition temperature. Polymer segmental relaxation and the

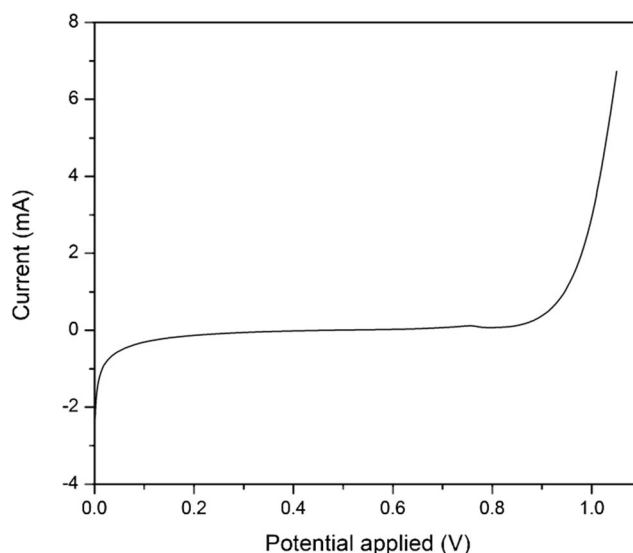
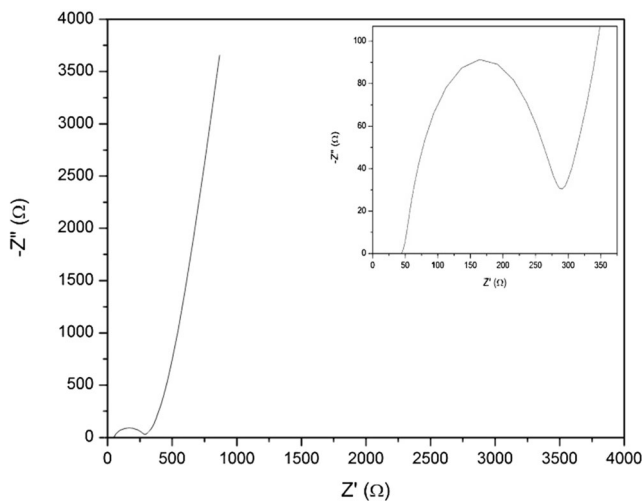


Fig. 5 Linear sweep voltammograms to determine the potential window of the electrolyte



**Fig. 6** The Nyquist plot for the full range of frequency and the high-frequency plot obtained for the EDLC

increase of the free volume cause the curvature shape of the VTF behavior [15].

Since the plot shows a straight line, the presence of the Arrhenius behavior can be observed from this study as illustrated in Fig. 3.

### Transference number measurements

Since SS electrodes are blocking ions, polarization of the ions take place initially and cause the rapid drop of the current. The stable current is caused by the electrons which are not blocked by the electrodes. Figure 4 shows the resulted plot of the current variation with time. Calculated  $t_i$  is 0.72. This shows that GPE is more or less an ionic conductor.

### Electrochemical stability window

It is important to determine the stable potential range of an electrolyte before going into any kind of potential applications [16]. LSV was used here to determine the potential window of the electrolyte. Figure 5 shows the outcome of the LSV test. Thereby increasing the potential after 0.9 V, the current flow

**Fig 7** **a** The plot of  $C'(\omega)$  with respect to the logarithmic scale of frequency. **b** The plot of  $C''(\omega)$  with respect to the logarithmic scale of frequency

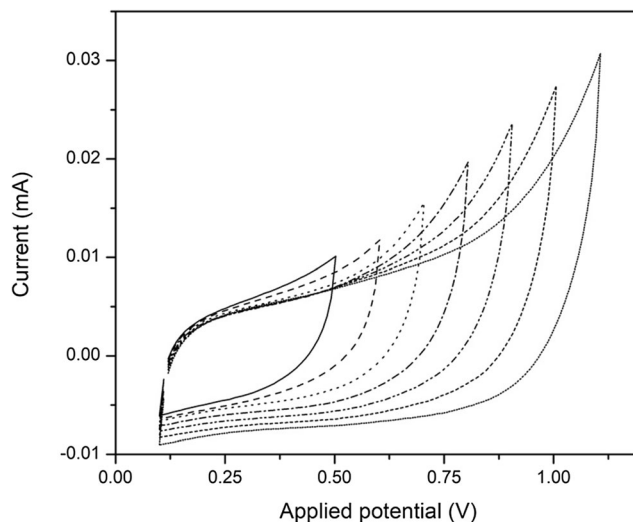
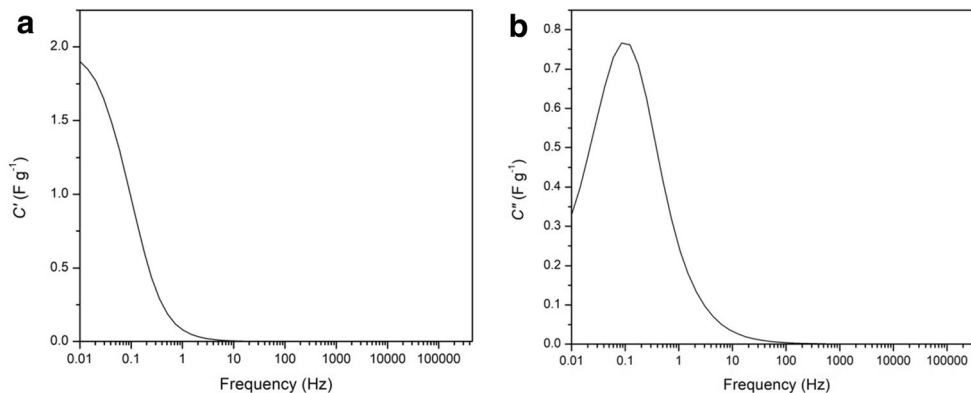


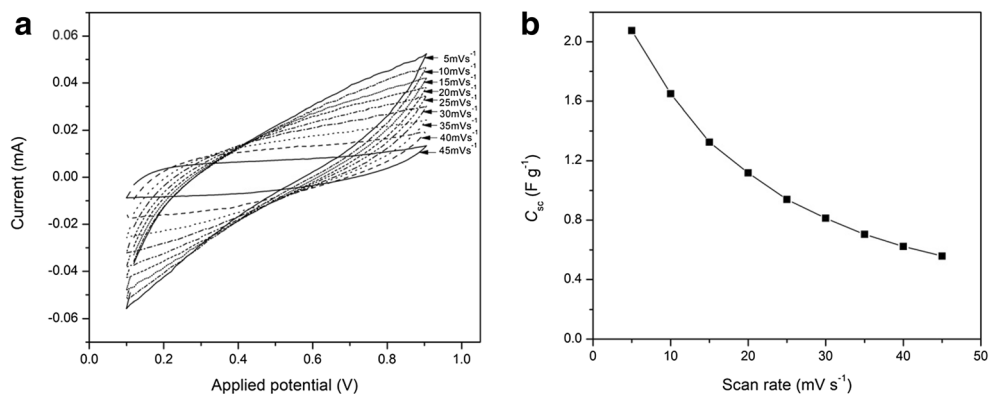
**Fig. 8** Cyclic voltammograms taken within various potential windows with  $10 \text{ mV s}^{-1}$  scan rate

began to increase dramatically which has the potential to damage to the electrolyte. Below 0.1 V, a drop of potential can be seen. Hence, the potential window from 0.1 to 0.9 V was taken as the stable potential range that can be applied on the system without a risk of damage to the electrolyte.

### Electrochemical impedance measurements for EDLCs

As shown in the Fig. 6, the Nyquist plot obtained for the EDLC has near semi-circle shape followed by a tilted spike when the frequency is decreased. The Nyquist plot of an ideal EDLC has two semi-circles at high- and mid-frequency ranges and a straight line at the low-frequency range which represent the internal resistance of the electrolyte, electrode electrolyte interface resistance, and capacitive behaviors, respectively [12]. In this study, it was not possible to observe the high-frequency semi-circle probably due to insufficient frequency range. The second semi-circle was not having the perfect semi-circular shape exhibiting the surface roughness and the poor contacts in between the electrolyte and the electrode surfaces [17]. Theoretically, the spike should be parallel to the  $Z''$ -axis if the

**Fig. 9** **a** Cyclic voltammograms taken with different scan rates within 0.1–0.9 V potential window. **b**  $C_{sc}$  variation with respect to the scan rate of the cyclic voltammograms



system shows pure capacitive features. Due to surface roughness of electrodes, a tilted spike can be present.

Figure 7a and b show the Bode plots of the real  $C'(\omega)$  and imaginary  $C''(\omega)$  parts of the complex capacitance as a function of frequency. The maximum  $C_{sc}$  corresponds to the maximum  $C'(\omega)$  and it is  $1.96 \text{ F g}^{-1}$ . A drastic drop of  $C_{sc}$  upon increasing frequency and eventually reaching to zero is observed in Fig. 7a; at lower frequencies, capacitive properties become dominant whereas resistive properties override capacitive properties with the increase of the frequency.

Relaxation time constant ( $\tau_R$ ) is a quantitative measure of the reversible charge–discharge rate of the EDLC and can be calculated using:

$$\tau_R = \frac{1}{2\pi f_0}$$

where frequency of maximum  $C''(\omega)$  occurs is  $f_0$  [18]. According to this, relaxation time constant of the device is 1.87 s indicating that ion transfer is fairly fast. This is an indication for existence of proper charging and discharging behavior of the fabricated device.

### Cyclic voltammetry test

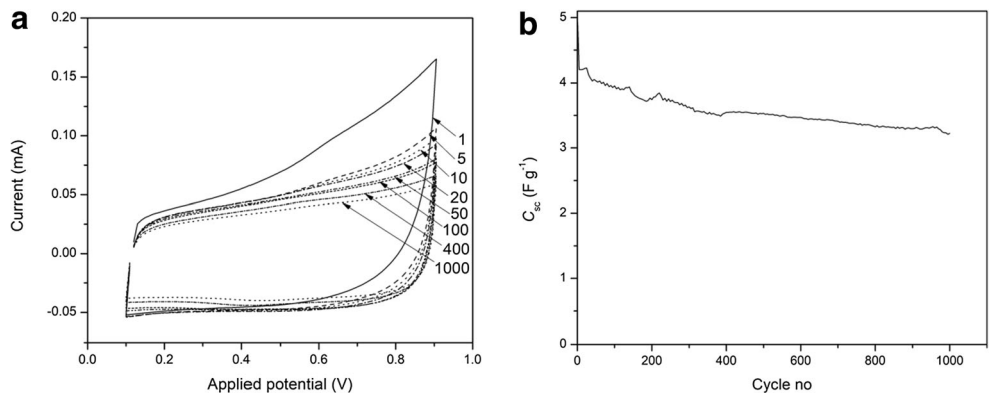
Figure 8 illustrates the cyclic voltammograms obtained for EDLC in various potential windows at the scan rate of  $10 \text{ mV s}^{-1}$ . All cyclic voltammograms obtained with a

minimum potential value of 0.1 V and consequently increased the maximum potential. When the width of the window increased beyond 1.0 V, the current through the device began to increase rapidly. This hints the unstable nature of the EDLC beyond that value. To avoid deterioration of the device that prefers a large number of charge–discharge cycles, the optimum window was taken as 0.1–0.9 V range. LSV results also backed up this potential window as explained before. Also, there were no distinct peaks appeared in any part of the window confirming that no redox reactions took place [19]. Since the charge storage mechanism at the carbon-based electrodes is not associated with any redox reaction, near rectangular shape of all cyclic voltammograms is a characteristic feature of an EDLC which involves accumulation of charges at the electrode/electrolyte system [6].

For the selected potential window of 0.1–0.9 V, scan rate was changed (Fig. 9a) and the  $C_{sc}$  was calculated simultaneously to find the optimum scan rate for the test.

Here, the lower scan rates such as  $5 \text{ mV s}^{-1}$  has the potential to give excessive  $C_{sc}$  values compared with higher scan rates as shown in the Fig. 9b. But the higher scan rates were much preferred since they complete the cycles faster in addition to the reduction of side reactions which may cause unnecessary accumulations, surface structural changes, and chemical depositions [20]. Therefore,  $20 \text{ mV s}^{-1}$  was chosen as the optimum scan rate for the continuous cycling since it has a considerably higher capacitance.

**Fig. 10** **a** Cyclic voltammograms from the continuous cycling test. **b** Variation of the single-electrode specific capacitance of cyclic voltammograms with the cycle number



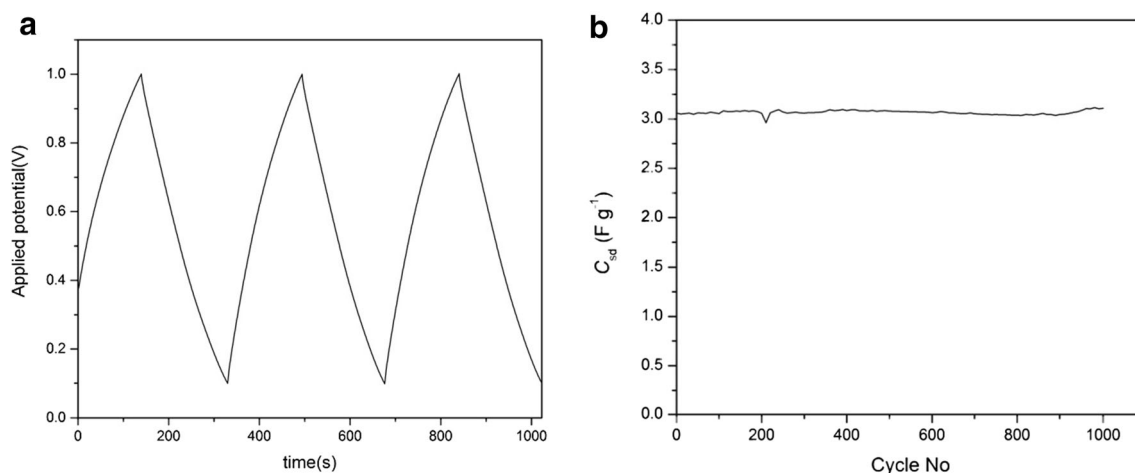


**Fig. 11** **a** Few charge–discharge cycles obtained from the GCD test. **b** The graph of the variation of specific discharge capacity with the cycle number

Continuous cycling of an EDLC is one of the important considerations in practical applications. Figure 10 a depicts the resulting cyclic voltammograms and Fig. 10 b shows  $C_{sc}$  variation with the cycle number using continuous CV test done within the potential window of 0.1 to 0.9 V and at the scan rate of  $20 \text{ mV s}^{-1}$ .

$C_{sc}$  of the EDLC was  $4.92 \text{ F g}^{-1}$  initially and decreased with the cycle number as in general. After 1000 cycles, it was about  $3.22 \text{ F g}^{-1}$ .  $C_{sc}$  retention was therefore turned out to be above 65%, and the decrease of  $C_{sc}$  could cause due to loss of interfacial reactions between the electrode and electrolyte and also due to degradation of electrolyte and/or electrodes [21].

### Galvanostatic charge–discharge test

Figure 11a illustrates few GCD cycles obtained, and  $C_{sd}$  calculated from constant charging and discharging with respect to the cycle number is illustrated in Fig. 11b.

Pattern of the cycles during charging and discharging are almost symmetric. And change of charge–discharge procedures at the set potentials takes place without any deviation. This guarantees the absence of any parasitic reactions. The  $C_{sd}$  at the first cycle was found to be  $3.06 \text{ F g}^{-1}$ , and for the whole 1000 cycles, it was nearly at a constant value. The steady capacitive behavior of the fabricated EDLC can be confirmed with the result [22]. There is a small drop and a regain of the  $C_{sd}$  can be observed around 200th cycle. This may be caused by side reactions, and the regain can be explained through the self-healing property of polymer electrolytes [23].

### Conclusions

The optimum composition of GPE was found as 26% PVdF-co-HFP:52%  $\text{ZnCl}_2$ :22% 1E3MICl by weight. When the IL concentration increases above 22%, the conductivity began to

decrease and further increase caused the membrane to deform. The conductivity variation with respect to the temperature shows the Arrhenius behavior. From the DC polarization test, the  $t_i$  was found to be 0.72 and the stable potential window was from 0 to 0.9 V by LSV.

An EDLC with the configuration graphite/1E3MICl-based GPE/graphite was fabricated successfully at room temperature. Impedance results reveal a maximum  $C_{sc}$  of  $1.96 \text{ F g}^{-1}$  with  $\tau_R$  of 1.87 s. The continuous CV test was done in the optimized potential window of 0.1 to 0.9 V at a scan rate of  $20 \text{ mV s}^{-1}$ . The  $C_{sc}$  of the EDLC was about  $4.92 \text{ F g}^{-1}$  and its retention was above 65% over 1000 cycles. The initial  $C_{sd}$  at the first cycle of the GCD test was found to be  $3.06 \text{ F g}^{-1}$  and was nearly constant for 1000 cycles. Moreover, the EDLC has a good stability and its degradation during the cycling is negligible. This can be used as an energy storage device in the future with further developments, and more studies will enhance the performance of the device.

**Funding information** The authors received assistance from the National Science Foundation, Sri Lanka (RG/2017/BS/02, RG/2015/EQ/07).

### Compliance with ethical standards

**Conflict of interest** The authors declare that they have no conflict of interest.

### References

1. Long L, Wang S, Xiao M, Meng Y (2016) Polymer electrolytes for lithium polymer batteries. *J Mater Chem A* 4(26):10038–10069
2. Cheng X, Pan J, Zhao Y, Liao M, Peng H (2017) Gel polymer electrolytes for electrochemical energy storage. *Adv Energy Mater* 8(7):1702184(1–16)
3. Singh PK, Bhattacharya B, Mehra RM, Rhee HW (2011) Plasticizer doped ionic liquid incorporated solid polymer electrolytes for photovoltaic application. *Curr Appl Phys* 11(3):616–619

4. Prasadini KW, Perera KS, Vidanapathirana KP (2018) 1-Ethyl-3-methylimidazolium trifluoromethanesulfonate-based gel polymer electrolyte for application in electrochemical double-layer capacitors. *Ionics* 25:2805–2811
5. Kumar D, Hashmi SA (2010) Ionic liquid based sodium ion conducting gel polymer electrolytes. *Solid State Ionics* 181(8–10):416–423
6. Du X, Guo P, Song H, Chen X (2010) Graphene nanosheets as electrode material for electric double-layer capacitors. *Electrochim Acta* 55(16):4812–4819
7. Syahidah SN, Majid SR (2015) Ionic liquid-based polymer gel electrolytes for symmetrical solid-state electrical double layer capacitor operated at different operating voltages. *Electrochim Acta* 175:184–192
8. Kim JI, Choi Y, Chung KY, Park JH (2017) A structurable gel-polymer electrolyte for sodium ion batteries. *Adv Funct Mater* 27(34):1701768(1–7)
9. Kuma M, Tiwari T, Srivastava N (2012) Electrical transport behaviour of bio-polymer electrolyte system: potato starch + ammonium iodide. *Carbohydr Polym* 88(1):54–60
10. Tey JP, Careem MA, Yarmo MA, Arof AK (2016) Durian shell-based activated carbon electrode for EDLCs. *Ionics* 22(7):1209–1216
11. Bandaranayake CM, Yayathilake YMCD, Perera KS, Vidanapathirana KP, Bandara LRAK (2016) Investigation of a gel polymer electrolyte based on polyacrylonitrile and magnesium chloride for a redox capacitor. *Ceylon J Sci* 45(1):75–82
12. Mei BA, Munteshari O, Lau J, Dunn B, Pilon L (2018) Physical interpretations of Nyquist plots for EDLC electrodes and devices. *J Phys Chem C* 122(1):194–206
13. Ravindran D, Vickraman P (2012)  $Mg^{+2}$  ionic conductivity behavior of mixed salt system in PVA-PEG blend matrix. *Int J Sci Res Publ* 2(12):1–4
14. Gong SD, Huang Y, Cao HJ, Lin YH, Li Y, Tang SH, Wang MS, Li X (2016) A green and environment-friendly gel polymer electrolyte with higher performances based on the natural matrix of lignin. *J Power Sources* 307:624–633
15. Ramesh S, Yi LJ (2009) Structural, thermal, and conductivity studies of high molecular weight poly(vinylchloride)-lithium triflate polymer electrolyte plasticized by dibutyl phthalate. *Ionics* 15(6):725–730
16. Kasnatscheew J, Streipert B, Roser S, Wagner R, Cekic LI, Winter M (2017) Determining oxidative stability of battery electrolytes: validity of common electrochemical stability window (ESW) data and alternative strategies. *Phys Chem Chem Phys* 19(24):16078–16086
17. Wang H, Shi Y, Cai N (2013) Effects of interface roughness on a liquid-Sb-anode solid oxide fuel cell. *Int J Hydrog Energy* 38(35):15379–15387
18. Zhao G, Zhang N, Sun K (2013) Porous  $MoO_3$  films with ultra-short relaxation time used for supercapacitors. *Mater Res Bull* 48(3):1328–1332
19. Roldán S, González Z, Blanco C, Granda M, Menéndez R, Santamaría R (2011) Redox-active electrolyte for carbon nanotube-based electric double layer capacitors. *Electrochim Acta* 56(9):3401–3405
20. Allagui A, Freeborn TJ, Elwakil AS, Maundy BJ (2016) Reevaluation of performance of electric double-layer capacitors from constant-current charge/discharge and cyclic voltammetry. *Sci Rep* 6:1–8
21. Kobayashi Y, Shono K, Kobayashi T, Ohno Y, Tabuchi M, Oka Y, Nakamura T, Miyashiro H (2017) A long life 4 V class lithium-ion polymer battery with liquid-free polymer electrolyte. *J Power Sources* 341:257–263
22. Amarsa SN, Kufian MZ, Majid SR, Arof AK (2011) Preparation and characterization of magnesium ion gel polymer electrolytes for application in electrical double layer capacitors. *Electrochim Acta* 57:91–97
23. Zhou B, Zuo C, Xiao Z, Zhou X, He D, Xie X, Xue Z (2018) Self-healing polymer electrolytes formed via dual-network: a new strategy for flexible lithium metal batteries. *Chem Eur J* 24(72):19200–19207

**Publisher's note** Springer Nature remains neutral with regard to jurisdictional claims in published maps and institutional affiliations.